IOP Publishing | Royal Swedish Academy of Sciences Physica Scripta
Phys. Scr. **T160** (2014) 014026 (6pp) doi:10.1088/0031-8949/2014/T160/014026

A detailed description of the experimental realization of a quantum illumination protocol

E D Lopaeva[1,2], I Ruo Berchera[1], S Olivares[3,4], G Brida[1], I P Degiovanni[1] and M Genovese[1]

[1] INRIM, Strada delle Cacce 91, I-10135 Torino, Italy
[2] DISAT, Politecnico di Torino, I-10129 Torino, Italy
[3] Dipartimento di Fisica, Università degli Studi di Milano, I-20133 Milano, Italy
[4] CNISM UdR Milano Statale, I-20133 Milano, Italy

E-mail: m.genovese@inrim.it

Received 3 July 2013
Accepted for publication 23 August 2013
Published 2 April 2014

Abstract
In this paper we propose and realise a practical quantum enhanced sensing protocol aimed at the detection of a partially reflecting object in a lossy and noisy environment. Our scheme is inspired by the theoretical quantum illumination protocol elaborated by Lloyd (2008 *Science* **321**, 1463) and Tan *et al* (2008 *Phys. Rev. Lett.* **101**, 253601). We demonstrate that when only photon counting is allowed our quantum protocol performs astonishingly better than the best classical counterpart.

Keywords: quantum illumination, entanglement, quantum correlations, quantum enhanced measurements

(Some figures may appear in color only in the online journal)

1. Introduction

In recent years, exploitation of the specific properties of quantum states has disclosed the possibility of realising tasks beyond classical limits, creating the new field of quantum technologies [1–11]. Among them, quantum metrology and imaging aim at improving the sensitivity and/or resolution of measurements exploiting non-classical features such as squeezing and quantum correlations (entanglement and discordant states) [12–16]. Nevertheless, in most of the realistic scenarios losses and noise are known to nullify the advantage of adopting quantum strategies [17, 18]. In this paper we describe in detail the first experimental realisation of a quantum illumination protocol aimed at detecting an object in a noisy environment. It preserves a strong advantage over the classical counterparts even in the presence of large amounts of noise and losses. The experiment, inspired by the theoretical ideas elaborated on in [19–22] (see also [23, 24]), has been performed exploiting only photon number correlations in twin beams. Thus, for its simplicity it can find widespread use. Even more importantly, it challenges the common belief that real application of quantum technologies is limited by their fragility to noise and losses.

In our scheme [25] for target detection a probe beam of a bipartite correlated state may be partially reflected by an object toward a camera, which also receives a thermal field acting as a noisy unknown background (a thermal bath). Our goal is to investigate the performances of the quantum protocol, in a detection framework in which only photon numbers (i.e. intensities) are measured, with respect to the best classical counterpart, namely a classically correlated light-based protocol. We show that the use of simple second-order correlation measurements already suffices in guaranteeing strong advantages to the quantum protocol. This represents fundamental progress toward a practical realisation with respect to some previous similar theoretical proposals [20, 21, 26], stemming from the 'quantum illumination' (QI) scheme of [19], where the discrimination strategy, based on the quantum Chernoff bound [27, 28], was very challenging from an experimental point of view.

We point out that the two fundamental starting points in the present work are the photon number/intensity measurement and the *a priori* unknown background. The latter means that a reliable independent measurement only on the background is forbidden. In other words, it is impossible to establish a reference threshold of photocounts (i.e. the mean

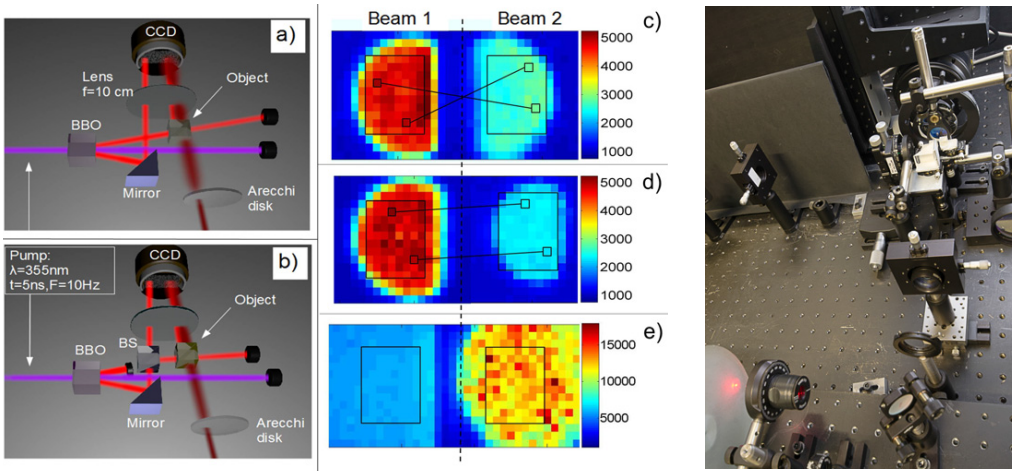

Figure 1. Experimental setup. (a) QI; (b) CI; (c) detected TWB, in the presence of the object, without thermal bath. The region of interest is selected by an interference filter centered around the degeneracy wavelength (710 nm) and bandwidth of 10 nm. After selection the filter is removed; (d) detected field for split THB in the presence of the object, without thermal bath; and (e) a typical frame used for the measurement, where the interference filter has been removed and a strong thermal bath has been added on the object branch. The color scales on the right correspond to the number of photons per pixel. On the right-hand side there is a photo of the set-up.

value of the background) to be compared with the possible additional mean photocounts coming from the reflected probe beam (if the target is present). Therefore, the estimation of the first-order (mean values) of the photocount distribution would be not informative regarding the presence or absence of the object. This unknown-background hypothesis accounts for a scenario where background properties can randomly change and drift with time and space. As a simple example one can consider either a single measurement through a hole of the presence of an object in a room with no information on the room lighting or of an object moving on a background whose illumination is unknowingly fluctuating. Therefore, the signal revealing the presence of the object must be extracted by measuring the higher orders of the joint photon number distribution, namely the photon number/ intensity correlation between the probe and a reference beam. We realize quantum target detection both by using QI, specifically twin beams (TWB), and by using classical illumination (CI), e.g. correlated thermal beams (THB), representing the best classical state in the specific detection framework, pointing out unequivocally the experimental advantage of the quantum protocol in the mesoscopic regime, independent of the noise level. The realization of the QI protocol, beyond paving the way to future practical applications, also provides a significant example of an ancilla-assisted quantum protocol in addition to previous ones, e.g. [16, 29–31]. As a first application of QI to QKD, with a different detection scheme, refer to the recent paper [32].

2. The experimental setup

In our setup (figure 1) correlated photon pairs in orthogonal polarizations are generated in a parametric down conversion (PDC) process by pumping a BBO (beta-barium-borate) nonlinear crystal with the third harmonic (355 nm) of a Q-switched Nd–Yag laser (repetition rate of 10 Hz, 5 ns pulse width) after spatial filtering. The correlated emissions are then addressed to a high quantum efficiency (about 80%, at 710 nm) CCD camera. The exposure time of the camera is set to collect in a single image the emission generated by a single laser shot. For the QI protocol (figure 1(a)) after the BBO crystal, where TWB are generated, one of the beams (the 'ancilla') is reflected toward the detection system. The correlated beam is partially detected, together with the thermal field from the Arecchi's disc, when the object (actually a beam splitter) is present, otherwise it is lost (did not show). Low-pass filter (95% of transmission at 710 nm) and UV-reflecting mirror are used to minimize the background noise while maintaining low losses. A lens, placed at the focal length from the crystal and the CCD camera, realizes the Fourier transform of the field at the output face of the crystal. The PDC light is then combined at the CCD with a thermal background (wavelength of 785 nm) produced by scattering a laser beam on an Arecchi's rotating ground glass. When the object is removed, only the thermal bath reaches the detector. In order to implement CI protocol (figure 1(b)), the TWB are substituted with classical correlated beams. These are obtained by splitting a multi-THB (single arm of PDC) and by setting the pump intensity to ensure equivalent intensity, time and spatial coherence properties for the quantum and the classical sources.

We note that traveling wave PDC generates a spatial multimode emission in the far field, where each mode corresponds to the transverse component of a specific wavevector. Each pair of correlated modes, corresponding to an opposite transverse component of the wavevector with respect to the pump direction, are found in symmetric positions [33]. Thus, we choose two correlated regions of interest (ROIs) on the CCD array (shown in figures 1(c)–(e)). The proper sizing of the pixels and the centering of the two-dimensional array with sub-mode precision, allows to maximize the collection of the correlated photons for each pair of pixels and at the same time to minimize the possible presence of uncorrelated ones [34]. In our experiment,

the correlation in the photon number, even at the quantum level for QI, is realized independently for each pair of symmetrical (translated) pixels that belong to the ROIs of the TWB (THB). Therefore, a single image is enough to evaluate correlation parameters, like covariance, averaging over the $N_{\rm pix}$ pairs ($N_{\rm pix} = 80$ pixels of size $A_{\rm pix} = (480\,\mu{\rm m})^2$). Albeit not strictly necessary, this is practically effective because it reduces the measurement time (less images are needed) and avoids to deal with the power instability of the pump laser from pulse to pulse, which is very destructive in this kind of application [35]. The number of spatio-temporal modes collected by a pixel is estimated to be $M = 9 \times 10^4$ by fitting a multithermal statistics. The average number of PDC photon per mode is $\mu = 0.075$. We measured separately the size of the spatial mode, as the full-width at half-maximum of the correlation function between the two beams, $A_{\rm corr} = (120 \pm 20\,\mu{\rm m})^2$. Thus, the number of spatial modes is about $M_{\rm sp} = A_{\rm pix}/A_{\rm corr} = 16 \pm 5$ and the number of temporal modes $M_{\rm t} = M/M_{\rm sp} = (6 \pm 2) \times 10^3$, the latter being consistent with the ratio between the pump pulse duration and the expected PDC coherence time, i.e. 1 ps. The statistics of the thermal background, in particular the number of collected temporal modes, can be adjusted by setting the ratio between the rotating speed of the disc and the duration of the pulse.

3. The model of the measurement

In our approach, the ability to distinguish the presence/absence of the object depends on the possibility of distinguishing between the two corresponding values of covariance $\Delta_{1,2}$ between the photon number N_1 and N_2 of a pair of correlated pixels, evaluated experimentally as

$$\Delta_{1,2} = E[N_1 N_2] - E[N_1]E[N_2], \tag{1}$$

where the quantity $E[X] = \frac{1}{\mathcal{K}} \sum_{k=1}^{\mathcal{K}} X^{(k)}$ represents the average over the set of $\mathcal{K}$ realizations corresponding in our experiment to the pixels of the ROI, i.e. $\mathcal{K} = N_{\rm pix} = 80$. Therefore, each image provides a determination of the covariance. Then we define the signal to noise ratio (SNR) of the counting base QI protocol as the ratio of the mean 'contrast' to its standard deviation (mean fluctuation)

$$f_{\rm SNR} \equiv \frac{\left|\left\langle \Delta_{1,2}^{\rm (in)} - \Delta_{1,2}^{\rm (out)} \right\rangle\right|}{\sqrt{\left\langle \delta^2\left(\Delta_{1,2}^{\rm (in)}\right)\right\rangle + \left\langle \delta^2\left(\Delta_{1,2}^{\rm (out)}\right)\right\rangle}}, \tag{2}$$

where 'in' and 'out' refer to the presence and absence of the object, respectively, and $\langle \cdots \rangle$ is the quantum expectation value. From equation (1) it follows that $\langle \Delta_{1,2} \rangle = (1 - \mathcal{K}^{-1}) \langle \delta N_1 \delta N_2 \rangle$ and, for $\mathcal{K} \gg 1$, $\langle \delta^2 \Delta_{1,2} \rangle \simeq \langle \delta^2 [\delta N_1 \delta N_2] \rangle / \mathcal{K}$. These expressions allow to calculate $f_{\rm SNR}$ theoretically. In particular the denominator can be calculated as

$$\mathcal{K} \left\langle \delta^2 \Delta_{1,2} \right\rangle \simeq \left\langle \delta^2 (\delta N_1 \delta N_2) \right\rangle \equiv \left\langle (\delta N_1 \delta N_2)^2 \right\rangle - \langle \delta N_1 \delta N_2 \rangle^2 . \tag{3}$$

By replacing $\delta N_2 \mapsto \delta N_2^{\rm (in)} + \delta N_{\rm b}$ where $N_2^{\rm (in)}$ is the number of detected photons that has been reflected by the target and $N_{\rm b}$ is the uncorrelated background, the right-hand side of (3) can be rewritten as

$$\begin{aligned} \mathcal{K} \langle \delta^2 \Delta_{1,2} \rangle &\simeq \left\langle \left(\delta N_1 \delta N_2^{\rm (in)} + \delta N_1 \delta N_{\rm b} \right)^2 \right\rangle \\ &\quad - \left\langle \delta N_1 \delta N_2^{\rm (in)} + \delta N_1 \delta N_{\rm b} \right\rangle^2 \\ &= \left\langle \left(\delta N_1 \delta N_2^{\rm (in)} \right)^2 \right\rangle - \left\langle \delta N_1 \delta N_2^{\rm (in)} \right\rangle^2 + \left\langle \delta^2 N_1 \right\rangle \left\langle \delta^2 N_{\rm b} \right\rangle \\ &= \left\langle \delta^2 (\delta N_1 \delta N_2^{\rm (in)}) \right\rangle + \left\langle \delta^2 N_1 \right\rangle \left\langle \delta^2 N_{\rm b} \right\rangle , \end{aligned} \tag{4}$$

where we used the statistical independence of $N_{\rm b}$ and the fact that $\langle \delta N_{\rm b} \rangle = 0$. It is clear that in the absence of the target (the situation labeled with the superscript 'out'), $N_2^{\rm (in)} = 0$, thus $\langle \delta^2 \Delta_{1,2}^{\rm (out)} \rangle = \left\langle \delta^2 N_1 \right\rangle \left\langle \delta^2 N_{\rm b} \right\rangle$, since nothing is reflected to the detector. However, if the background fluctuation $\left\langle \delta^2 N_{\rm b} \right\rangle$ is the largest contribution to the noise, also when the target is present (indicated with superscript 'in') we can write $\langle \delta^2 \Delta_{1,2}^{\rm (in)} \rangle \simeq \left\langle \delta^2 N_1 \right\rangle \left\langle \delta^2 N_{\rm b} \right\rangle$. Under this assumption representing a realistic situation of a very noisy environment, the SNR becomes

$$f_{\rm SNR} \simeq \frac{\langle \delta N_1 \delta N_2 \rangle}{\sqrt{2 \left\langle \delta^2 N_1 \right\rangle \left\langle \delta^2 N_{\rm b} \right\rangle}}. \tag{5}$$

We underline that (5) holds for a dominant background, irrespective of its statistics (e.g. multi-thermal or Poissonian).

In our experiment we consider background with multi-thermal statistics. For a generic multi-thermal statistics with a number of spatiotemporal modes M, a mean photon number per mode μ, the total number of detected photons is $\langle N \rangle = M \eta \mu$ and the mean squared fluctuation is $\left\langle \delta^2 N \right\rangle = M \eta \mu (1 + \eta \mu) = \langle N \rangle \left(1 + \langle N \rangle / M\right)$ (see for example [36]), where η is the detection efficiency.

Thus, the amount of noise introduced by the background can be increased by boosting its total number of photons $\langle N_{\rm b} \rangle$ or by varying the number of modes $M_{\rm b}$.

Moreover, both TWB and correlated THB present locally the same multi-thermal statistics, but with a number of spatiotemporal modes $M = 9 \times 10^4$ much larger than the one used for the background beam ($M_{\rm b} = 57$ in one case and $M_{\rm b} = 1.3 \times 10^3$ in the other). This contributes to making the condition of preponderant background effective in our realization, even for a relatively small value of $N_{\rm b}$.

However, we point out that all the theoretical curves reported in all the figures are evaluated by the exact analytical calculation of the fourth-order (in the number of photons) quantum expectation values appearing on the right-hand side of (3), even if the whole expressions are far more complex than the ones obtained with the assumption of a preponderant background.

Starting from (5) and considering the same local resources for classical and QI beams (in particular the same local variance $\left\langle \delta^2 N_i \right\rangle_{\rm CI} = \left\langle \delta^2 N_i \right\rangle_{\rm QI}$ ($i = 1, 2$)) the enhancement of the quantum protocol can be easily obtained as

$$R = \frac{f_{\rm SNR}^{\rm (QI)}}{f_{\rm SNR}^{\rm (CI)}} \approx \frac{\langle \delta N_1 \delta N_2 \rangle_{\rm QI}}{\langle \delta N_1 \delta N_2 \rangle_{\rm CI}} = \frac{\varepsilon^{\rm (QI)}}{\varepsilon^{\rm (CI)}}. \tag{6}$$

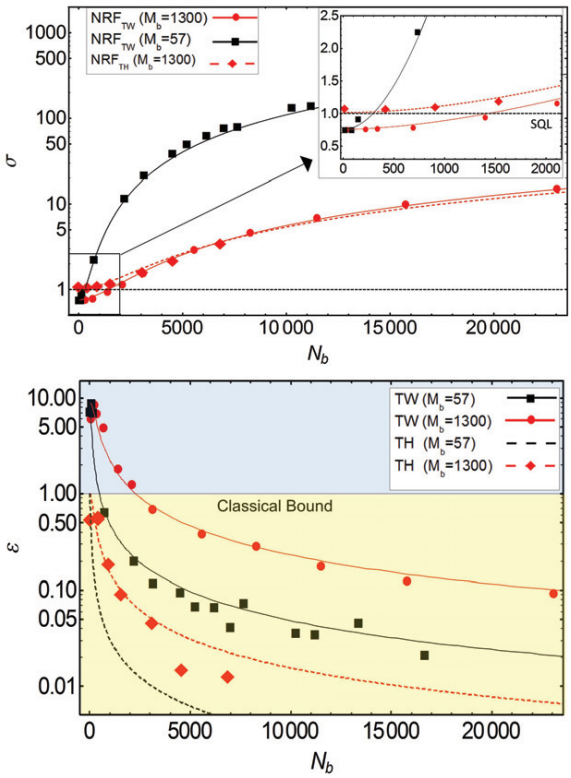

Figure 2. Top: NRF in the case of TWB, $\mathrm{NRF_{TW}}$, and of the correlated THB, $\mathrm{NRF_{TH}}$, as a function of the average number of background photons N_b for $M_\mathrm{b} = 57$ (black series) and $M_\mathrm{b} = 1300$ (red). The lines represent the theoretical prediction for $\eta_1 = 2\eta_2 = 0.4$ and $\mu = 0.075$ (the latter estimated independently). For $N_\mathrm{b} = 0$, $\mathrm{NRF_{TW}}$ is $\sigma = 0.761 \pm 0.006$. Statistical uncertainty bars are too small to be visible. Bottom: generalized Cauchy–Schwarz parameter ε in the case of TWBs, $\varepsilon^{(\mathrm{TW})}$, and of the correlated THB, $\varepsilon^{(TH)}$, as a function of the average number of background photons N_b for a number of background modes $M_\mathrm{b} = 57$ (black series) and $M_\mathrm{b} = 1300$ (red). The lines represent the theoretical prediction at $\mu = 0.075$ (the last estimated independently).

with $\varepsilon = \langle : \delta N_1 \delta N_2 : \rangle / \sqrt{\langle : \delta^2 N_1 : \rangle \langle : \delta^2 N_2 : \rangle}$ being the generalized Cauchy–Schwarz parameter, where $\langle : \ : \rangle$ is the normally ordered quantum expectation value. This parameter is interesting since it does not depend on the losses and it quantifies non-classicality being $\varepsilon \leqslant 1$ for the classical state of light (with positive P-function). The covariance of two correlated beams obtained by splitting a single THB is $\langle \delta N_1 \delta N_2 \rangle_\mathrm{TH} = M \eta_1 \eta_2 \mu_\mathrm{TH}^2$, while the one of TWB is $\langle \delta N_1 \delta N_2 \rangle_\mathrm{TW} = M \eta_1 \eta_2 \mu_\mathrm{TW} (1 + \mu_\mathrm{TW})$ (see e.g. [12]). By using this relation with the assumption of the same local resources, $\mu_\mathrm{TH} = \mu_\mathrm{TW} = \mu$ we can derive explicitly $R \approx (1 + \mu)/\mu$, which is insensitive to the amount of noise and loss. On the other side the generalized Cauchy–Schwarz parameter for a split THB is $\varepsilon_0^{(\mathrm{CI})} = 1$, where the subscript '0' stands for 'in the absence of background', as it can be easily derived from the equations of covariance and single beam fluctuations used previously. Therefore the comparison with split THB represents the comparison with the 'best' classical case.

4. Results

First of all we evaluate the noise reduction factor (NRF) defined as [16, 34, 37, 38]

$$\sigma \equiv \frac{\langle \delta^2 (N_1 - N_2) \rangle}{\langle N_1 + N_2 \rangle}, \tag{7}$$

where $\langle N_i \rangle$ is the mean value and $\delta^2 N_i = (N_i - \langle N_i \rangle)^2$ is the fluctuation of the photon number N_i, $i = 1, 2$, detected by correlated pixels. It represents the noise of the photon number difference normalized to the shot noise level or standard quantum limit [34]. For classical states $\sigma \geqslant 1$, while it is always smaller than 1 for TWB. In particular, when the thermal bath is off, we have $\sigma_0 = 1 - \overline{\eta} + (\eta_1 - \eta_2)^2 (1/2 + \mu) / (2\overline{\eta})$, with $\overline{\eta} = (\eta_1 + \eta_2)/2$, and η_i is the overall detection efficiency of beam $i = 1, 2$ [34, 35]. It includes all the transmission-detection losses, thus $\eta_1 = 2\eta_2$ due to the presence of the half reflecting object in the path of the second beam. In figure 2 we report the measured NRF and the theoretical prediction. From the inset one can observe that the NRF is actually in the quantum regime ($\sigma < 1$) for small values of the thermal bath, and in absence of it we obtain $\sigma_0 = 0.76$ corresponding to $\eta_1 = 0.4$. While, as soon as the contribution of the bath to the fluctuation of N_2 becomes dominant, NRF increases quite quickly, well above the classical threshold. As expected from the multi-thermal character of the bath, the number of modes M_b determines the noise level introduced, and it can be tuned easily according to the spin velocity of the ground-glass disc and/or the acquisition time. We also note that, for THB, the NRF is always in the classical regime.

As a second figure of merit, more appropriate for quantifying the quantum resources exploited by our QI strategy, we consider the generalized Cauchy–Schwarz parameter ε introduced in section 3. In figure 2 we report the measured ε and the theoretical prediction. One observes that for TWB $\varepsilon^{(\mathrm{QI})}$ is actually in the quantum regime ($\varepsilon^{(\mathrm{QI})} > 1$) for small values of the thermal background $\langle N_\mathrm{b} \rangle$ ($\varepsilon_0^{(\mathrm{QI})} \simeq 10$ when $\langle N_\mathrm{b} \rangle = 0$). Also here, $\varepsilon^{(\mathrm{QI})}$ decreases quite quickly, well below the classical threshold with the intensity of the background. As expected, for THB $\varepsilon^{(\mathrm{CI})}$ is always in the classical regime (being one for $\langle N_\mathrm{b} \rangle = 0$).

In figure 3, the $f_\mathrm{SNR}/\sqrt{\mathcal{K}}$ is compared with the experimental data, where the estimation of quantum mean values of (2) are obtained by performing averages of $\Delta_{1,2}^{(\mathrm{in/out})}$ over a set of N_img acquired images. While the SNR unavoidably decreases with the added noise for both QI and CI, the ratio between them is almost constant ($R \gtrsim 10$) regardless of the value of N_b, in agreement with the results of section 3. In turn, the measurement time, i.e. the number of repetitions N_img needs for discriminating the presence/absence of the target, is dramatically reduced (for instance, to achieve $f_\mathrm{SNR} = 1$, N_img is 100 times smaller when quantum correlations are exploited). Furthermore, figure 3 shows that the mean value of the covariance does not depend on the quantity of environmental noise, because, as expected, only the correlated components survive to this operation. However, the added noise influences drastically the uncertainty on the measurement for a certain fixed

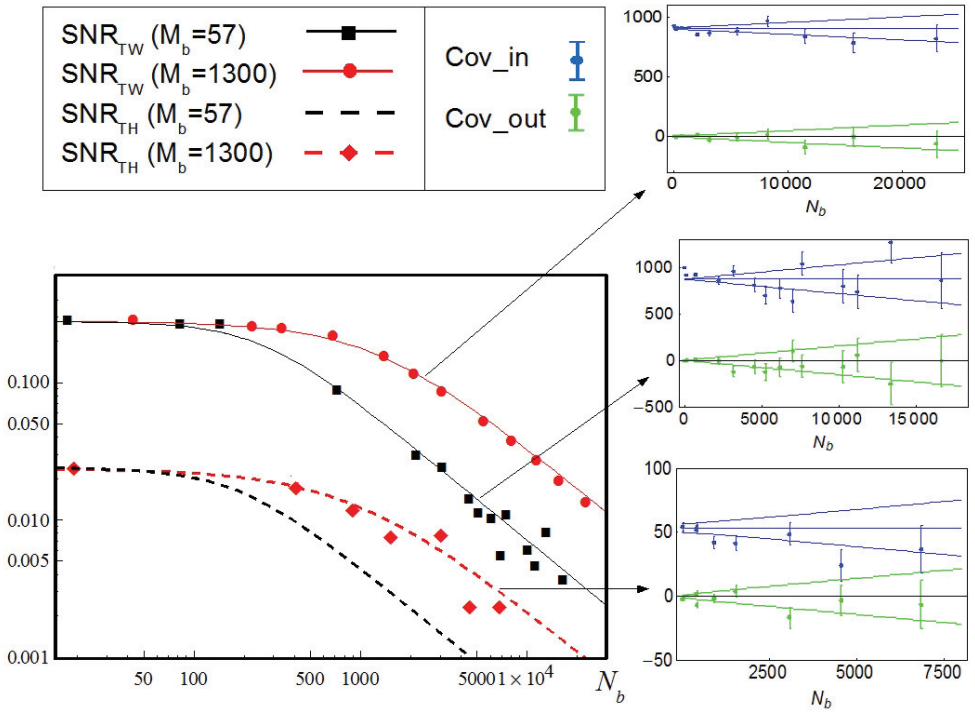

Figure 3. SNR versus N_b normalized by the square root of number of realization. The red (black) markers refer to $M_b = 1300$ ($M_b = 57$) and the solid (dashed) theoretical curve corresponds to quantum (classical) illuminating beams. The lowest curve of the classical protocol has not been compared with the experimental data because the SNR is so low that a very large number of images (out of the possibility of the actual setup) is required to have reliable points. The insets on the right present the covariance values corresponding to the three data sets indicated by the arrows. The blue (green) color refers to the data when the object is present, $\Delta_{1,2}^{(in)}$ (absent $\Delta_{1,2}^{(out)}$). The uncertainty bars represent the uncertainty of the mean values of the covariance obtained averaging over the N_{img} images (from the top to bottom: $N_{img} = 2000$, 6000 and 4000). Horizontal lines are the theoretical values $\langle\Delta_{1,2}^{(in/out)}\rangle$, while the uncertainty bars should be compared with the gap between the dashed lines, corresponding to the theoretically evaluated $\langle\delta^2\Delta_{1,2}^{(in/out)}\rangle/\sqrt{N_{img}}$.

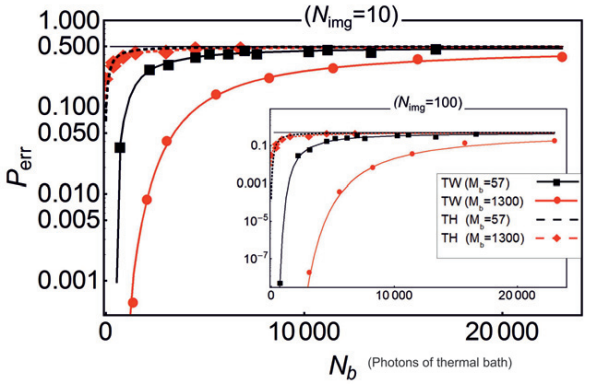

Figure 4. Error probability P_{err} of the target detection versus the total number of photons of the thermal bath N_b evaluated with $N_{img} = 10$ ($N_{img} = 100$ in the inset). The black squares and red circles are the data for QI with $M_b = 57$ and 1300, respectively, while red diamonds refers to the data for the CI with $M_b = 1300$. The curves are the corresponding theoretical predictions.

number of images N_{img} and thus the ability to assert the presence of the object.

In order to show that the quantum strategy outperforms the classical one, in figure 4 we report the error probability in the discrimination, P_{err}, versus the number of photons of the thermal bath N_b. The statement on the presence/absence of the object is performed on the basis of the covariance value obtained for a fixed number of images $N_{img} = 10$. Thus, P_{err} is estimated by fixing the threshold value of the covariance that minimizes the error probability itself. Figure 4 shows a remarkable agreement between the theoretical predictions (lines) and the experimental data (symbols), both for QI and CI strategy. Furthermore, the P_{err} in the case of QI is several orders of magnitude below the CI one and, in terms of background photons, the same value of the error probability is reached for a value of N_b at least ten times larger than in the QI case.

5. Conclusions

We have described in detail the model and the experiment which addresses quantum enhancement in detecting a target in a thermal radiation background in a relevant and realistic measurement scenario. Our system shows quantum correlation with no external noise ($\sigma = 0.76$) even in the presence of the losses introduced by the only partially reflective target. Remarkably, even after the transition to the classical regime ($\sigma \gg 1$), the scheme preserves the same strong advantage with respect to its natural classical counterpart based on classically correlated beams, as also suggested in [20]. This apparent contradiction is explained by considering that quantum correlations actually survive

unchanged up to the detector, where they are simply added to an independent noisy background. Moreover the quantum resources and the quantum enhancement achieved by the protocol can be precisely quantified by the generalized Cauchy–Schwarz parameter that is only related to the source properties ε.

Unlike other quantum-enhanced measurement protocols, based on the experimental estimation of the first moments of the photon number distribution, our scheme, which is based on the measurement of the second-order momenta, is impressively robust against losses. This derives from the fact that it does not require a high level of two-mode squeezing ($\sigma_0 = 0.76$ in our experiment). For instance the quantum imaging protocol [16], where the signal is given by $\langle N_1 - N_2 \rangle$, provides a maximum improving factor of $1/\sqrt{\sigma_0}$ over classical techniques, that would correspond to 1.14 in our working condition in the absence of thermal background. Also in exemplar quantum-enhanced schemes, such as the detection of small beam displacement [14] and phase estimation by interferometry [17], it is well-known that losses and noise can rapidly decrease the advantage of using quantum light [18], and typically a high level of squeezing is necessary. This has enforced within the generic scientific community the common belief that the advantages of entangled and quantum states are hardly applicable in a real context, and they will remain limited to proofs of principle experiments in highly controlled laboratories, and/or to mere academic discussions. Our work challenges this belief by demonstrating an advantage of orders of magnitude with respect to CI protocol, independent of the amount of thermal noise and using devices currently available. In summary, we believe that the photon counting-based QI protocol has a huge potential to foster the exploitation of quantum light-based technologies in real lossy and noisy environments.

Acknowledgments

The research leading to these results has received funding from the EU FP7 under grant agreement no. 308803 (BRISQ2), from the EU under the project EMRP projects EXL02-SIQUTE Fondazione SanPaolo and MIUR (FIRB 'LiCHIS'—RBFR10YQ3H, Progetto Premiale 'Oltre i limiti classici di misura').

References

[1] Bouwmeester D *et al* 1997 *Nature* **390** 575
[2] Ursin R, Jennewein T, Aspelmeyer M, Kaltenbaek R, Lindenthal M, Walther P and Zeilinger A 2004 *Nature* **430** 849
[3] Boschi D, Branca S, De Martini F, Hardy L and Popescu S 1998 *Phys. Rev. Lett.* **80** 1121
[4] O'Brien J L 2007 *Science* **318** 1567
[5] Yao X C *et al* 2012 *Nature* **482** 489
[6] Yamamoto T, Koashi M, Özdemir S K and Imoto N 2003 *Nature* **421** 343
[7] Pan J W, Simon C, Brukner C and Zeilinger A 2001 *Nature* **410** 1067
[8] Pan J W, Gasparoni S, Ursin R, Weihs G and Zeilinger A 2003 *Nature* **423** 417
[9] Ruo Berchera I, Degiovanni I P, Olivares S and Genovese M 2013 *Phys. Rev. Lett.* **110** 213601
[10] Brida G, Castelletto S, Degiovanni I P, Genovese M, Novero C and Rastello M L 2000 *Metrologia* **37** 629
[11] Brida G, Degiovanni I P, Florio A, Genovese M, Giorda P, Meda A, Paris M and Shurupov A 2010 *Phys. Rev. Lett.* **104** 100501
[12] Brida G *et al* 2011 *Phys. Rev. A* **83** 063807
[13] Kolobov M I 2007 *Quantum Imaging* (New York: Springer)
[14] Treps N, Grosse N, Bowen W P, Fabre C, Bachor H A and Lam P K 2003 *Science* **301** 940
[15] Boyer V, Marino A M, Pooser R C and Lett P D 2008 *Science* **321** 544
[16] Brida G, Genovese M and Ruo Berchera I 2010 *Nature Photon.* **4** 227
[17] Giovannetti V, Lloyd S and Maccone L 2011 *Nature Photon.* **5** 222–9
[18] Thomas-Peter N, Smith B J, Datta A, Zhang L, Dorner U and Walmsley I A 2011 *Phys. Rev. Lett.* **107** 113603
[19] Lloyd S 2008 *Science* **321** 1463
[20] Tan S-H, Erkmen B I, Giovannetti V, Guha S, Lloyd S, Maccone L, Pirandola S and Shapiro J H 2008 *Phys. Rev. Lett.* **101** 253601
[21] Shapiro J H and Lloyd S 2009 *New J. Phys.* **11** 063045
[22] Guha S and Erkmen B I 2009 *Phys. Rev.* A **80** 052310
[23] Sacchi M F 2005 *Phys. Rev.* A **71** 062340
[24] Sacchi M F 2005 *Phys. Rev.* A **72** 014305
[25] Lopaeva E D, Ruo Berchera I, Degiovanni I P, Olivares S, Brida G and Genovese M 2013 *Phys. Rev. Lett.* **110** 153603
[26] Shapiro J 2009 *Phys. Rev.* A **80** 022320
[27] Audenaert K M R, Calsamiglia J, Muñoz-Tapia R, Bagan E, Masanes L, Acin A and Verstraete F 2007 *Phys. Rev. Lett.* **98** 160501
[28] Calsamiglia J, Muñoz-Tapia R, Masanes L, Acin A and Bagan E 2008 *Phys. Rev.* A **77** 032311
[29] Brida G, Ciavarella L, Degiovanni I P, Genovese M, Migdall A, Mingolla M G, Paris M G A, Piacentini F and Polyakov S V 2012 *Phys. Rev. Lett.* **108** 253601
[30] Takahashi H, Wakui K, Suzuki S, Takeoka M, Hayasaka K, Furusawa A and Sasaki M 2008 *Phys. Rev. Lett.* **101** 233605
[31] Altepeter J B, Branning D, Jeffrey E, Wei T C, Kwiat P G, Thew R J, O'Brien J L, Nielsen M A and White A G 2003 *Phys. Rev. Lett.* **90** 193601
[32] Zhang Z, Tengner M, Zhong T, Wong F N C and Shapiro J H 2013 *Phys. Rev. Lett.* **111** 010501
[33] Brambilla E, Gatti A, Bache M and Lugiato L A 2004 *Phys. Rev.* A **69** 023802
[34] Brida G, Genovese M, Meda A and Ruo Berchera I 2011 *Phys. Rev.* A **83** 033811
[35] Brida G, Degiovanni I P, Genovese M, Rastello M L and Ruo Berchera I 2010 *Opt. Express* **18** 20572
[36] Mandel L and Wolf E 1995 *Optical Coherence and Quantum Optics* (Cambridge: Cambridge University Press)
[37] Bondani M, Allevi A, Zambra G, Paris M G A and Andreoni A 2007 *Phys. Rev.* A **76** 013833
[38] Iskhakov T, Chekhova M V and Leuchs G 2009 *Phys. Rev. Lett.* **102** 183602